The 5th European sCO_2 Conference for Energy Systems
March 14–16, 2023, Prague, Czech Republic

2023-sCO2.eu-128

OPTIMISATION OF THE AIR CHANNELS ON THE DIVERSE ULTIMATE HEAT SINK FOR SCO2 POWER CYCLES

Radomír Filip
Research center Řež
Husinec-Řež, Czech Republic
Email: radomir.filip@cvrez.cz

Sarah Tioual-Demange
Fives Cryo
Golbey, France

Guillaume Taiclet
Fives Cryo
Golbey, France

ABSTRACT

During the Horizon 2020 sCO2-4-NPP project, several key components for the sCO_2 power cycle as an option for the innovative decay heat removal system for nuclear power plants were developed. One of them was the diverse ultimate heat sink (DUHS), which is an air/sCO_2 plate and fin heat exchanger with straight fins. A representative DUHS mock-up was manufactured and its thermal–hydraulic performance was tested using the sCO2 loop at Research Centre Rez (CVR) at parameters of 8 MPa of pressure and temperatures up to 170°C on the sCO2 side. The main findings were the acquisition of the heat transfer correlation on the air side of the heat exchanger and the fanning friction factor in the tiny channels. The collected data were used to verify the heat exchanger design and, moreover, a mathematical model was developed and validated. Furthermore an optimisation study was done using the validated model to find the best channel geometry with the trade-off between high heat transfer coefficient and low pressure losses.

INTRODUCTION

In the framework of the Horizon 2020 sCO2-4-NPP project [1], where the goal was to utilise the self-sustaining sCO2 power cycle to serve as an additional safety system within the current nuclear power plants, to remove the decay heat during a station blackout (SBO) scenario, several key components were developed. The key components of such a system are schematically shown in Figure 1. These are the compact heat exchanger, turbomachinery and air-cooled diverse ultimate heat sink (DUHS).

The work presented in this paper is focused on the heat removal between the sCO2 and the ambient air, which is mediated in the DUHS. The DUHS is required to cool the sCO2 from 240°C down to 55°C at 8 MPa pressure to maintain the cycle functionality, even at some extreme ambient conditions <-45; 45°C>, while maintaining low pressure losses and having light and compact design. To meet these requirements, a plate and fin heat exchanger (PFHE) design with straight fins was proposed and a 500 kW unit was designed. The preliminary design of the DUHS unit is 2 m in width, 0.64 m in length and 0.98 m in height. It contains 64 layers of sCO2 channels wound up into eight passes and 128 layers of straight-passage air channels (schematically shown in Figure 2). Where one layer of sCO2 is stacked between two air layers, the stacking pattern is known as 'double-banking' and it is schematically presented in Figure 3.

To validate the thermal–hydraulic design, a small DUHS mock-up unit was fabricated and tested, using the experimental sCO2 loop [2] at Research Centre Rez (CVR). The experimental data were used to extrapolate the heat transfer and fanning friction coefficient correlations. A special focus was placed on the air side of the DUHS, since the overall heat transfer coefficient is mainly governed by the heat transfer coefficient on the air side, due to the higher convective heat transfer resistance. Thus, improving the channel geometry on the air side would have major impact on the required heat transfer area. For this reason, a 1D numerical model was developed and validated with the experimental results, which was further employed for the optimisation study, that aims to get a channel geometry with an optimal trade-off between heat transfer coefficient and low pressure losses.

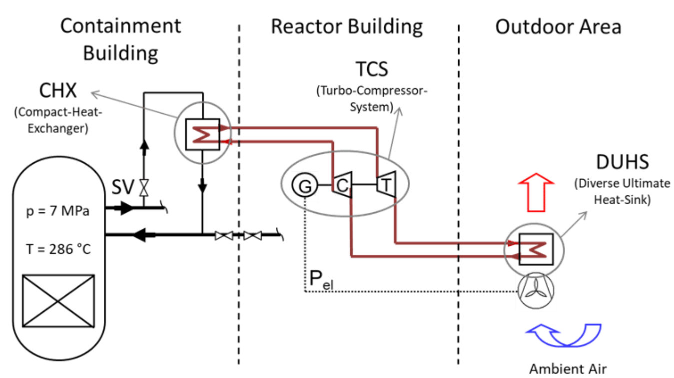

Figure 1: sCO2 heat removal system attached to a BWR [3].

DOI: 10.17185/duepublico/77298

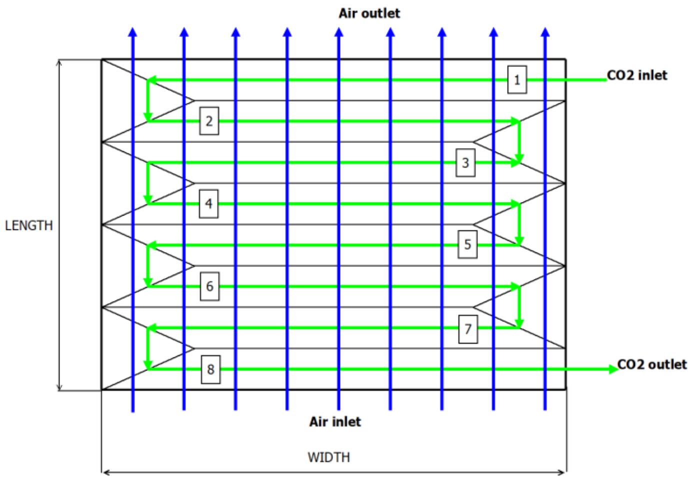

Figure 2: Scheme of DUHS core with cross flow configuration.

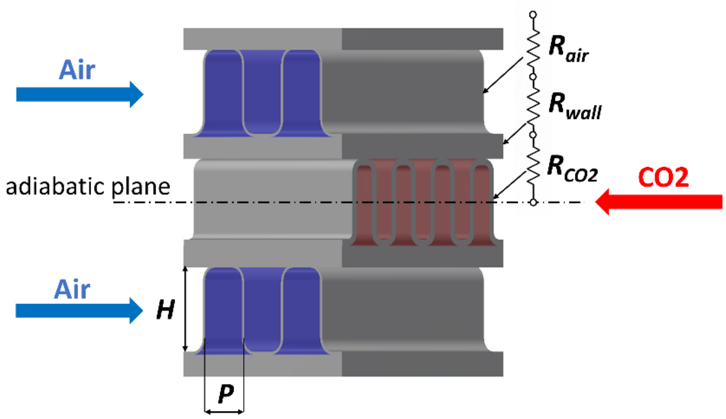

Figure 3: Scheme of DUHS channels 'double-banking' arrangement.

EXPERIMENTAL VERIFICATION

The fabricated DUHS mock-up (shown in Figure 4) is 305 mm in width, 224 mm in length and 52 mm in height and consists of three layers per CO2 side with four passes and effective passage length of 1.22 m and six layers per air side with effective passage length of 0.24 m. Each layer is separated with a 1 mm thick sheet made of stainless steel. The channels on the air side contain 0.15 mm thick fins with 2.54 mm spacing, and the sCO2 channels contain 0.3 mm thick fins with 1.27 mm spacing. The height of both channels is 4 mm. The heat exchanger testing took place at CVR using an sCO2 experimental loop, which was constructed within the SUSEN (Sustainable Energy) project [2]. The sCO2 loop is a large-scale experimental facility in the form of a simple Brayton cycle with a heating power of 110 kW, sCO2 temperatures up to 550°C, pressure up to 25 MPa and mass-flow rate up to 0.3 kg/s. The facility has been used within various R&D projects focused on the development of sCO2 cycles and components testing. The DUHS mock-up was implemented in the low-pressure part of the sCO2 loop, which corresponds to an appropriate location in the real sCO2 cycles.

For the experiments, the DUHS mock-up's air side was equipped with flange ducts on both sides, where the inlet side was connected to the blower and the outlet side was left to the ambient. The sCO2 side was connected to the low-pressure section of the sCO2 experimental loop, which was operated at 8 MPa with inlet temperatures in range of <100; 172°C>, to ensure the CO2 was above its critical point. The experimental PID layout is schematically shown in Figure 5. The installed instrumentations with their measurement errors are listed in Table 1. To minimize the thermal losses, the whole DUHS mock-up was for the experiments wrapped in 5cm thick thermal insulation.

Table 1: List of used instrumentation.

Variable	Description	Range	Units	Measurement error
T1,2,3	K-type Thermocouple class 1	0–300	°C	± 1.5°C
T4,5,6,7, 8,9,10,11	Pt100 class A	0–300	°C	± 0.35°C
F1	Thermic flow sensor	0–465	m3/h	± 5% of measured value
F2	Coriolis flow meter	0–0.7	kg/s	± 10% of measured value
P	Absolute pressure transducer	0-30	MPa	± 0.3 bar
PD1	Pressure difference transducer	0–15	mbar	± 0.1 mbar
PD2	Pressure difference transducer	0–500	mbar	± 0.4 mbar

Figure 4: Fabricated DUHS mock-up**.**

DOI: 10.17185/duepublico/77298

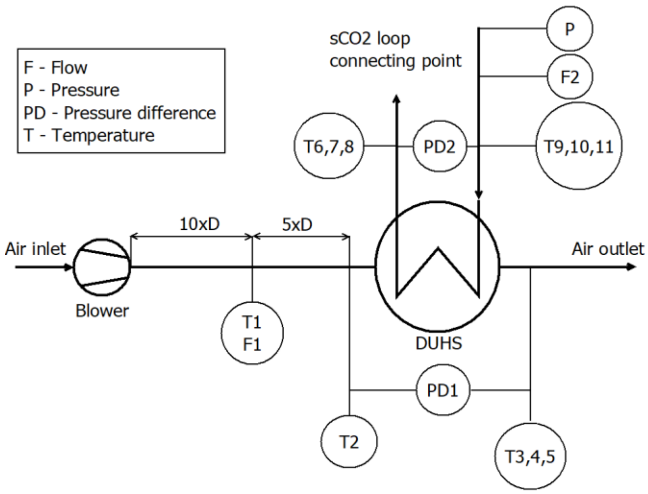

Figure 5: PID of the DUHS experimental setup.

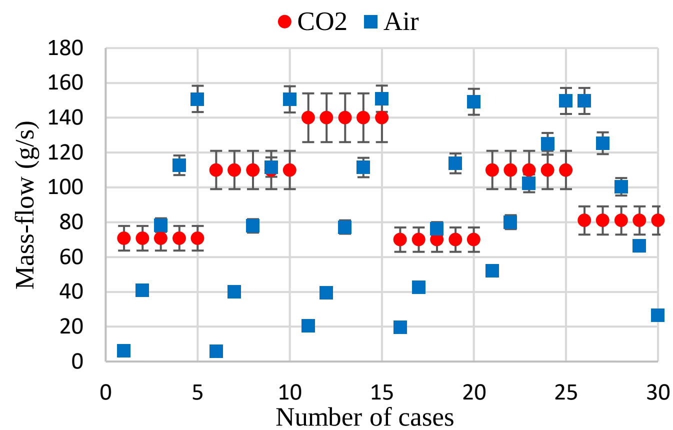

Figure 7: Experimental data: Mass-flow.

EXPERIMENTAL RESULTS

During the experimental campaign, the sCO2 mass-flow and inlet temperature were kept constant at six different levels, while the absolute pressure was kept at 8 MPa. Then for each sCO2 state, a different air mass-flow setting was applied at five different levels. Hence, a total of 30 steady state data points were obtained. Indicators for determining a steady state were the outlet temperatures gradients of both media. Where each data point was considered steady state when there was no significant temperature gradient change. Final inlet/outlet temperatures were obtained by averaging measured data at given location. As for example the outlet sCO2 temperature is considered as arithmetic average of measured values T6; T7; T8. The final averaged temperatures are present for each steady state in Figure 6. The measured mass-flows of both media are present in Figure 7 together with their range of measurement error bar given by the devices measurement error from Table 1. Furthermore the measured pressure drop for the sCO2 side and the air side are plotted in Figure 8 and Figure 9 respectively. The entire overview of the measured data is present for validation purposes in Appendix A.

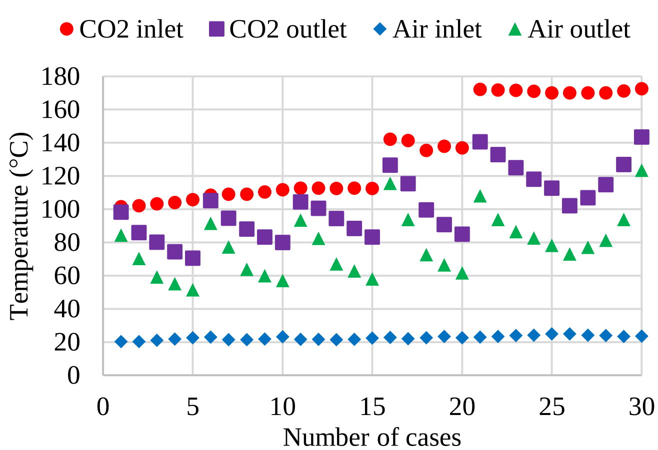

Figure 6: Experimental data: Temperatures.

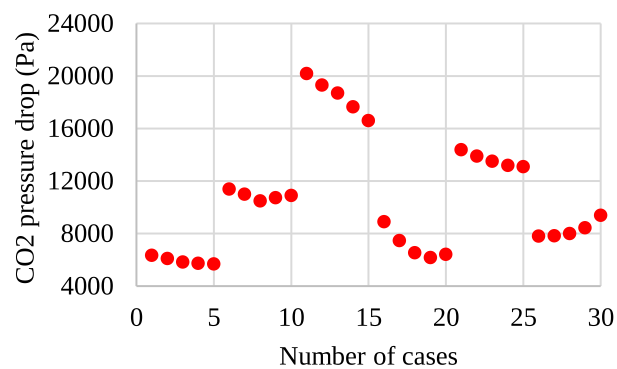

Figure 8: Experimental data: CO2 side pressure loss.

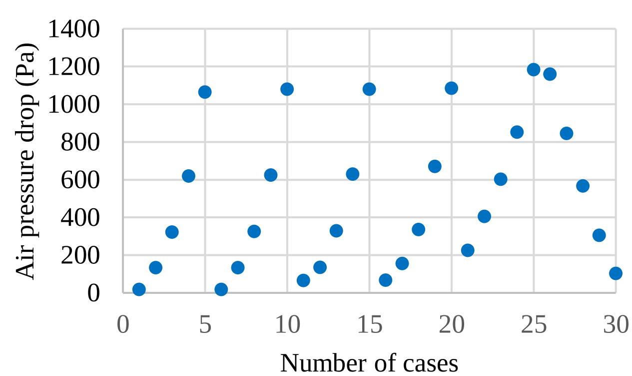

Figure 9: Experimental data: Air side pressure loss.

Heat transfer rate was calculated according to Eq. 1, using the measured mass-flow and the enthalpy difference between the inlet ant outlet for each medium. The enthalpies were obtained with NIST REFPROP [4], inputting the measured temperatures and pressures. In case of air, the ambient pressure of 1 bar was considered.

DOI: 10.17185/duepublico/77298

.

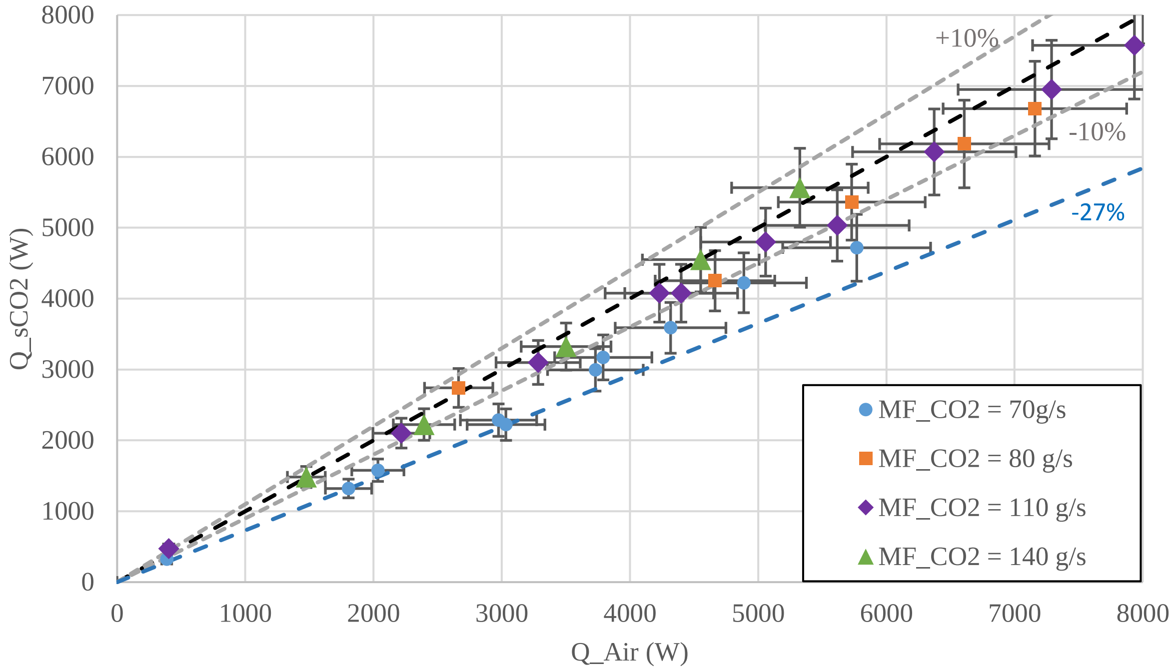

Figure 10: Calculated heat transfer rates according to the experimental results at different sCO2 mass-flow rates.

$$Q = \dot{m} \cdot \Delta i \quad (1)$$

The thermal losses were with respect to the used insulation, outer surface area and the highest temperature gradient estimated to be less than 1% of the average heat transfer rate and thus were neglected.
The heat transfer rate uncertainty σ_Q was considered as an error propagation function of three independent parameters (mass flow, inlet/outlet enthalpy). The error propagation function was linearized by approximation to a first order Taylor series expansion that can be calculated as follows:

$$\sigma_Q = \sqrt{(\Delta i \cdot \sigma_{\dot{m}})^2 + (\dot{m} \cdot \Delta\sigma_i)^2} \quad (2)$$

Where $\Delta\sigma_i$ is the enthalpy uncertainty difference between the values at the inlet and outlet. Each enthalpy uncertainty can be generally expressed as :

$$\sigma_i = \frac{\sqrt{\left(i_{(T,Pmax)} - i_{(T,Pmin)}\right)^2 + \left(i_{(Tmax,P)} - i_{(Tmin,P)}\right)^2}}{2} \quad (3)$$

The heat transfer rate error propagation was calculated in this manner for both media. Resulted heat transfer rates of both media with their errors are plotted in Figure 10, where it can be seen a black dashed line that stands for Q_{sCO2}/Q_{Air} = R = 1. Resulted sCO2 heat transfer, that was measured with mass-flows > 80g/s, lies within the range from R ± 10% (grey dashed lines). However it can be noted that the measured data with sCO2 mass-flow of 70g/s shows higher dispersion from R, up to -27% (blue dashed line). This seems to be problem of the Coriolis flow meter that is used to measure the sCO2 mass flow and its accuracy, measuring in range of less than 10% of its measure span. For this reason the total heat transfer rate is considered $Q_T = Q_{Air}$, when sCO2 mass flow is < 80g/s, when is above, the total heat transfer rate is consider as follows:

$$Q_T = 0.5\,(Q_{CO2} + Q_{Air}) \quad (4)$$

HEAT TRANSFER COEFFICIENT

The heat transfer coefficient on the air side can be expressed from the experimental data, knowing the heat transfer resistances, then the following expression is valid:

$$R_{air} = R_{tot} - R_{wall} - R_{CO2} \quad (5)$$

This can be written as:

$$R_{air} = \frac{LMTD}{Q_t} - \frac{t}{(kA)_{wall}} - \frac{1}{(\eta_0\, htc\, A)_{CO2}} \quad (6)$$

Assuming the sum of the thermal resistances R_{wall} and R_{CO2} is an order of magnitude smaller than the resulting thermal resistance on the air side of the heat exchanger, the overall heat transfer coefficient will be mainly affected by the heat transfer coefficient on the air side. Therefore, in order to determine the heat transfer coefficient on the sCO_2 side, some general *htc* correlation for

DOI: 10.17185/duepublico/77298

forced convection can be used. For this purpose, Gnielinsky correlation is used and is valid in the range $10^4 < Re < 10^6$ [5]:

$$htc = \frac{(\xi/8)RePr}{1 + 12.7\sqrt{(\xi/8)}(Pr^{2/3} - 1)} \cdot \left[1 + \left(\frac{D_h}{L}\right)^{2/3}\right]\left(\frac{k}{D_h}\right) \tag{7}$$

where ξ is defined as:

$$\xi = (1.8log_{10}Re - 1.5)^{-2} \tag{8}$$

Since the heat exchanger contains fins, the total heat transfer rate is evaluated through a concept of total surface effectiveness η_0 defined as :

$$\eta_0 = 1 - (1 - \eta_f)\frac{A_f}{A} \tag{9}$$

where A_f is the fin surface area and A is the total surface area, and η_f is the fin efficiency defined as:

$$\eta_f = \frac{\tanh(h'X)}{h'X} \tag{10}$$

where X is defined as:

$$X = \sqrt{\frac{2\,htc}{k_s\,t}} \tag{11}$$

The value of the *h'* term for the 'double-banking' pattern will differ for the air and CO_2 channel. In the case of the air channel, $h' = h - t$, but in the case of the CO_2 channel, the adiabatic plane is in the middle of the channel (shown in Figure 3), thus $h' = h/2 - t$.

The fin surface area A_f is considered as:

$$A_f = 2(H - t) \cdot L \cdot N \tag{12}$$

where *N* is the number of channels and *L* is their effective length. The total area is considered as:

$$A = 2(P - t) \cdot L \cdot N + A_f \tag{13}$$

Finally, the heat transfer coefficient on the air side can be calculated by iterating the following expression:

$$htc_{air} = \frac{1}{(\eta_0\,A\,R)_{Air}} \tag{14}$$

Obtained heat transfer coefficients are converted into the Colburn factor form according to [6]:

$$j = \frac{htc_{air}}{\rho\bar{v}c_p}Pr^{2/3} \tag{15}$$

The Colburn factor was correlated as a function of Reynolds number, using the least square linear regression method. The following function was found, to best match the extrapolated data:

$$j = 0.084 \cdot Re^{-0.47} \tag{16}$$

The stated Colburn factor correlation is valid for air and straight fins in the range of Reynolds numbers <500; 4000>. Figure 11 shows the extrapolated and correlated values of the Colburn factor coefficients as a function of the Reynolds number. The comparison of the correlated and the extrapolated data is shown in Figure 12, where the correlation matches the extrapolated data with an average absolute deviation of 6.1% and lies within the maximum error band of ± 15%.

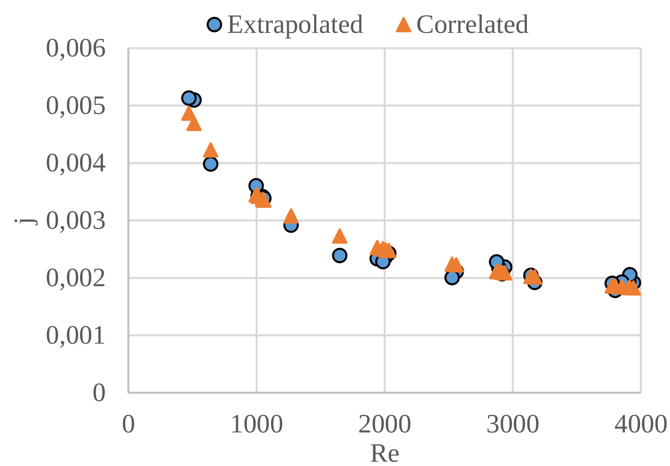

Figure 11: Colburn factor as a function of Reynolds number.

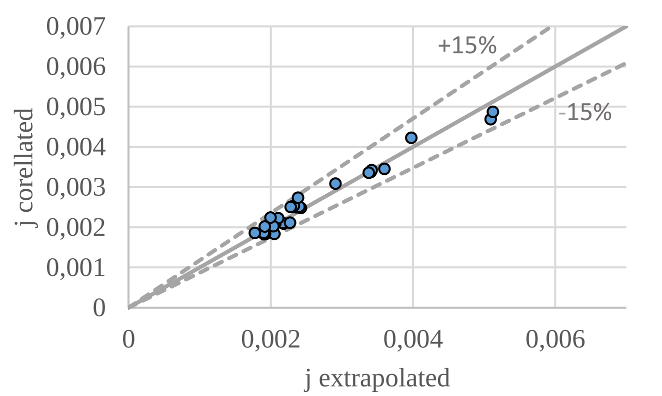

Figure 12: Correlation field between extrapolated and correlated Colburn factors**.**

FANNING FRICTION FACTOR

The fanning friction factor can be determined from the experimental data with the following equation [7]:

DOI: 10.17185/duepublico/77298

$$f = \frac{D_h}{2L}\frac{1}{(1/\rho)_m}\left[\frac{2\Delta p}{G^2} - \frac{1}{\rho_i}(1-\sigma^2+K_c) - 2\left(\frac{1}{\rho_o} - \frac{1}{\rho_i}\right) + \frac{1}{\rho_o}(1-\sigma^2+K_e)\right] \quad (17)$$

where σ is the contraction/expansion ratio, which is the ratio of the total front flow area over the total front area at the entrance/exit. Kc and Ke are entrance/exit friction factors that were determined from graph [8]. The fanning friction factor was calculated according to Eq. (13) and correlated using the least square linear regression method. The resulting correlation for the fanning friction factor on the air side is as follows:

For laminar region Re < 2000:

$$f = \frac{18.3}{Re} \quad (18)$$

For turbulent region 2000 < Re < 4000

$$f = 0.017\ Re^{-0.07} \quad (19)$$

The comparison between extrapolated and correlated friction factors is show in Figure 13. The correlation field is shown in Figure 14, where the average absolute deviation between extrapolated and correlated data is 5.3% and all the data lie within the maximum error band of ± 15%.

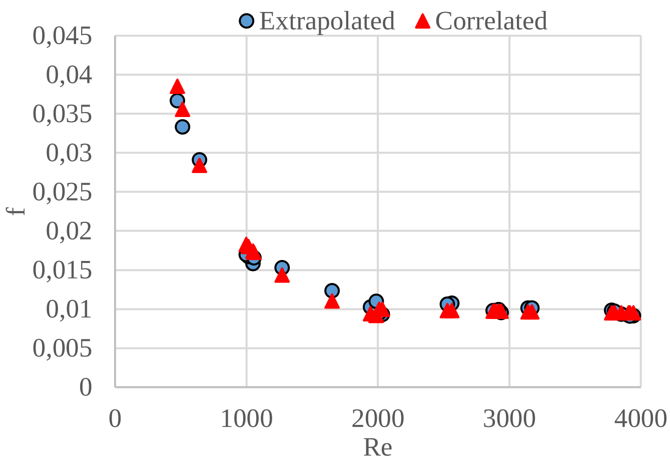

Figure 13: Friction factor as a function of Reynolds number.

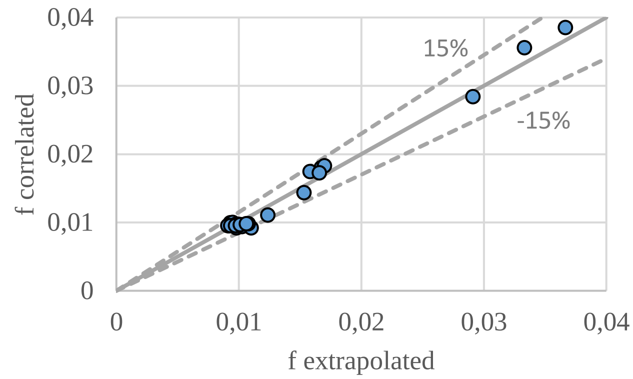

Figure 14: Friction factor as a function of Reynolds number.

MATHEMATICAL MODELLING

To validate the thermal–hydraulic performance of the DUHS mock-up and potential design of different channel geometries, a 1D mathematical model was developed, utilising the correlations obtained from the experimental results. To calculate the heat transfer, an ε-NTU method was employed [8]. The heat exchanger was discretised into smaller net transfer units, where the number of rows corresponds to the index *i*, which is equal to the number of sCO_2 passages, then the index *j* corresponds to the number of columns (shown in Figure 15). In this case, the flow arrangement can be considered as unmixed crossflow, where the heat exchanger effectiveness is given by expression:

$$\varepsilon = 1 - exp\left((\exp(-NTU^{0.78}W^*) - 1)NTU^{0.22} / W^*\right) \quad (20)$$

where *NTU* and W^* are given as follows:

$$NTU = \frac{UA_{i,j}}{W_{min}} \quad (21)$$

$$W^* = \frac{W_{min}}{W_{max}} \quad (22)$$

where *W* is a flow heat capacity rate with units (W/K). With the current arrangement, the minimal flow heat capacity will be, in this case, always at the air side; thus, the following expressions for the inlet/outlet NTU temperatures in the first row are valid:

$$T_{air(i+1,j)} = T_{air(i,j)} + \varepsilon_{(i,j)} \cdot (T_{CO2(i,j)} - T_{air(i,j)}) \quad (23)$$

$$T_{CO2(i,j+1)} = T_{CO2(i,j)} + W^* \cdot (T_{air(i+1,j)} - T_{air(i,j)}) \quad (24)$$

DOI: 10.17185/duepublico/77298

The temperatures are iteratively calculated in this manner until certain accuracy is reached. The thermo-physical properties of each medium were obtained from the NIST database [4] and are considered at the average inlet/outlet temperature of each NTU at constant operating pressure.
The mass-flows and flow heat capacities for each medium are calculated as:

$$\dot{m}_i = \frac{\dot{Q}}{\Delta i_i} \tag{25}$$

$$W_i = \frac{\dot{Q}}{\Delta T_i} \tag{26}$$

The DUHS geometrical parameters are listed in Table 2. The channel's *flow area,* the hydraulic diameter D_h and total number of channels N are calculated as:

$$Flow\ area_i = (P_i - t_i)(H_i - t_i) \tag{27}$$

$$D_{h_i} = 4 \cdot Flow\ area/(2((P_i - t_i) + (H_i - t_i))) \tag{28}$$

$$N_i = (FPM_i \cdot Effective\ width + 1) \cdot number\ of\ layers \tag{29}$$

The channel velocities and Reynolds numbers are calculated as:

$$v_i = \frac{\dot{m}_i}{Flow\ area_i\ \rho_i\ N_i} \tag{30}$$

$$Re_i = \frac{v_i\ D_{h_i}\ \rho_i}{\mu_i} \tag{31}$$

As for the heat transfer coefficients and the overall heat transfer coefficient, these can be calculated from Eq. (6), where the new heat transfer correlation was utilised. For the hydraulic calculation, Eq. (17) can be rewritten into the following form to obtain a formula for the pressure losses:

$$\Delta p = \frac{G^2}{2}\frac{1}{\rho_i}\left[(1-\sigma^2+K_c) + f\frac{2L}{D_h}\rho_i\left(\frac{1}{\rho}\right)_m + 2\left(\frac{\rho_i}{\rho_o} - 1\right) - \frac{\rho_i}{\rho_o}(1-\sigma^2+K_e)\right] \tag{32}$$

During the pressure loss calculations, the correlated fanning friction factors from Eq. (18) and Eq. (19) were used.

Table 2: DUHS mock-up - geometrical parameters.

	Air	sCO_2
FPM	388.2	787.4
P (mm)	2.576	1.27
H (mm)	4	4
t (mm)	0.2	0.3
number of layers	6	3
Effective width (mm)	281	50
Effective length (mm)	214	1,220

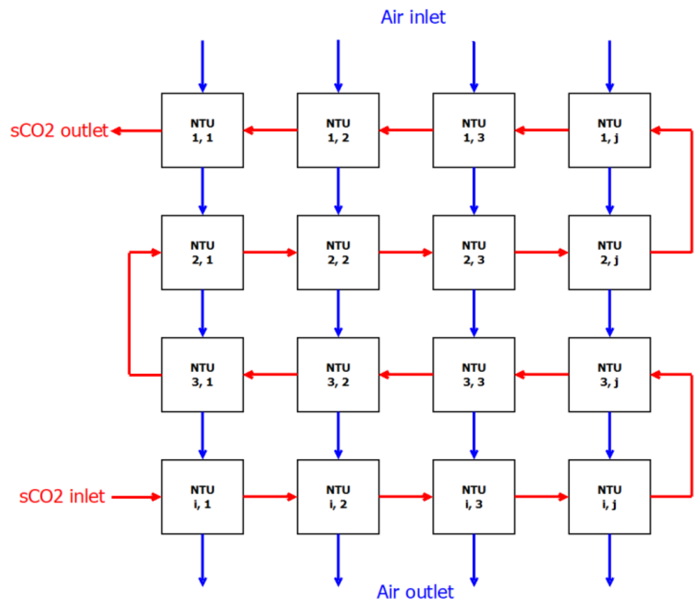

Figure 15: Discretisation of DUHS mock-up used in the ε-NTU method.

MATHEMATICAL MODEL RESULTS

To validate the numerical 1D model, it was fed with the measured experimental data, namely the total transferred heat Q_T, input/output CO_2 temperatures and input air temperature. For the heat transfer model validation, the air outlet temperatures predicted by the model and measured during the experiment were compared. The air outlet temperatures comparison is shown in Figure 16, where the predicted air outlet temperatures are matching the experimental data with reasonably good precision, where the predicted temperatures fit within ± 10% error band together with the measured values. The absolute average deviation, comparing measured and modelled data was 3.8%. Regarding the hydraulic model validation, the pressure differences on the air side, predicted by the model were compared with the experimental measurement. The comparison of the pressure difference on the air side is shown in Figure 17, where the predicted pressure losses fit within ± 30% error band. While comparing the measured and modelled data, the absolute average deviation was 11.8%. Slightly higher deviations of the pressure loss predictions on the air side are mainly caused by the initial uncertainty of the mass-flow measurements and resulting

DOI: 10.17185/duepublico/77298

calculation of the average heat transfer, which was the main model input. Despite this fact, the numerical model predicts the thermal and hydraulic performance reasonably well and can be considered valid.

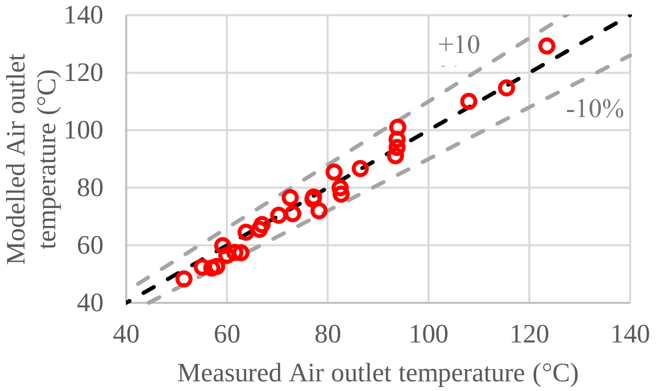

Figure 16: Comparison of the air outlet temperatures predicted by the model vs. measured values.

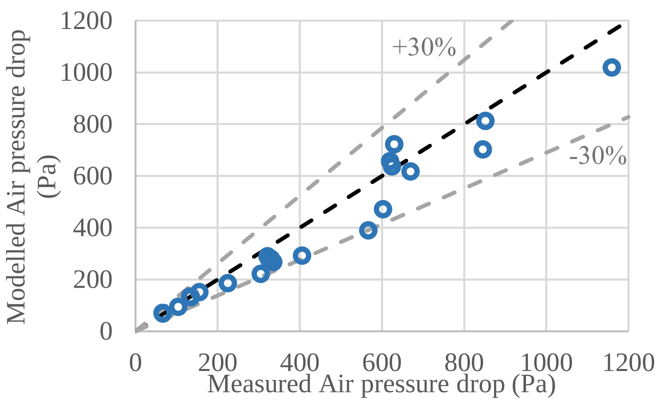

Figure 17: Comparison of the pressure difference on the air side predicted by the model vs. measured values.

AIR SIDE CHANNEL OPTIMISATION

An optimisation task was carried out in order to find a straight fin channel geometry that maintains a high heat transfer coefficient with low pressure losses. New heat transfer and friction factor correlations obtained from the experimental results were used for this purpose. The optimisation parameters are the pitch, height and thickness of the channel's fins. The limits for these parameters that are present in Table 3, were chosen according to the discussion with the HX manufacturer FIVES Cryo, where the manufacturability was the main consideration. For the optimisation task, a single channel was considered with the following constraints:

- channel length 1m
- constant flow velocity 8 m/s
- maximum allowable pressure 600 Pa/m
- constant air thermo-physical properties at mean temperature $T_m = 70°C$
- contraction/expansion ratio $\sigma = 0.5$

Table 3: Intervals of the air channel optimisation parameters.

Channel parameter	Interval (mm)
Pitch – P	<1; 5>
Height – H	<2; 8>
Fin thickness – t	<0.1; 0.3>

The velocity value of 8 m/s was chosen as a reasonable trade-off between heat transfer and pressure losses. The pressure loss limit of 600 Pa/m was chosen with respect to the flow characteristics of some commercial axial fans, which are characterised with high flow rates and lower static pressures.
A channel's hydraulic diameter for each possible combination of P(i), H(j) and t(k) was calculated as:

$$D_{h_{i,j}} = \frac{2 \cdot (P_i - t_k)\left(H_j - t_k\right)}{(P_i - t_k) + \left(H_j - t_k\right)} \tag{33}$$

An array of Reynolds numbers was obtained using Eq. (31), then the heat transfer coefficient was calculated as a function of the Reynolds number as follows:

$$htc_{i,j} = \frac{Re_{i,j}\, \mu\, c_p\, j}{D_{h_{i,j}}\, Pr^{2/3}} \tag{34}$$

where Eq. (16) was used to obtain the Colburn factor *j*. The pressure losses were calculated according to Eq. (32), where fanning friction factors from Eq. (18) and Eq. (19) were utilised. To find an optimum between high heat transfer coefficient and low pressure losses, a weight ratio system was utilised. The pressure losses were linearly scaled between values in <0; 1> , where the zero value was assigned to an array with value lower than the pressure loss limit of 600 Pa/m and a value of one was assigned to the minimum calculated pressure loss. The same was done with heat transfer coefficient, where one was considered the maximum calculated *htc* value and zero was considered the minimum *htc* in the array. This results in obtaining two arrays with values in the interval <0; 1>. The final weight was obtained by element-wise multiplication of the two arrays.

OPTIMISATION RESULTS

According to the results, an increase in given dimensions of the fin thickness has a positive effect on the fin efficiency (shown in Figure 18), which is projected into a slight increase of the effective heat transfer coefficient, presented in Figure 21. Hence, a fin thickness of 0.3 mm can be proposed for the channel design. Combining the smallest given pitch and height values, a maximum effective heat transfer coefficient of $htc = 41.7$ $W/m^2.K$ for the given boundary conditions can be reached.

DOI: 10.17185/duepublico/77298

However, this combination also contains a point with the highest calculated pressure loss, with a value of Δp = 3110 Pa, which exceeds the given allowable limit limit by a factor of five (shown in Figure 19). When utilising the weight ratio system with the maximum allowable pressure loss of 600 Pa/m, a surface contour is obtained, as shown in Figure 20. The presented surface has a visible hyperbolic ridge, where the final weight reaches its maximum. This zone represents an area with optimum trade-off between the heat transfer coefficient and sufficiently low pressure losses. The preliminary design point was marked on this surface alongside three other points lying near the region with a local maximum, shown in Figure 22. The values of the effective heat transfer coefficient and the pressure losses for each point, as well as the preliminary design point, are presented in Table 4. It can be noted that the preliminary design point has the highest value of the effective *htc* from the given points, namely 10.8% more than the average of the three points. However, the pressure loss is also the highest, at 35.4% more than the average. The differences of the values between the considered points are negligible; therefore, the final design can be proposed according to the matching aspect ratio H/P as the same geometry of the DUHS mock-up, where the experimental results were obtained and thus the results should match more closely. Hence, according to the data, the geometry at point two can be recommended for the future design.

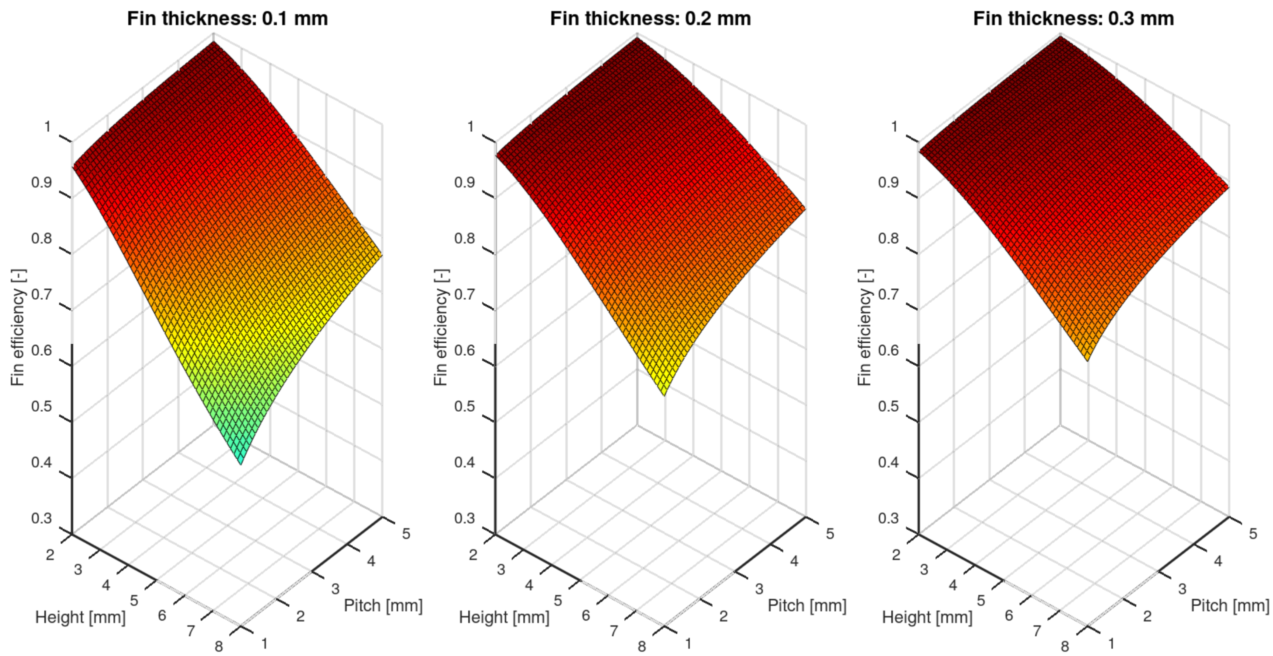

Figure 18: Comparison of a fin efficiency for different fin thicknesses (0.1; 0.2; 0.3 mm respectively).

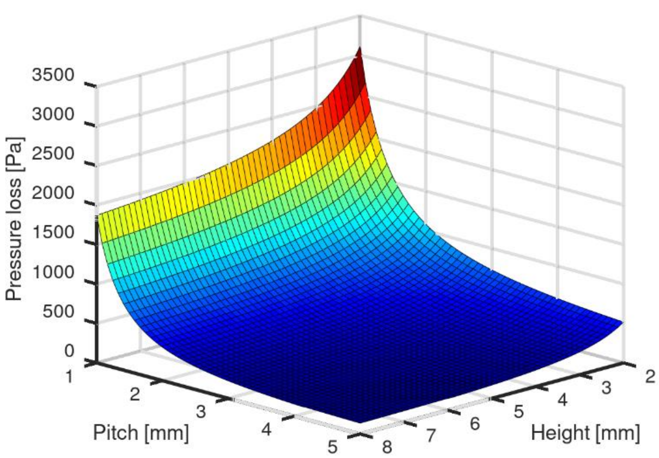

Figure 19: Pressure losses surface contour.

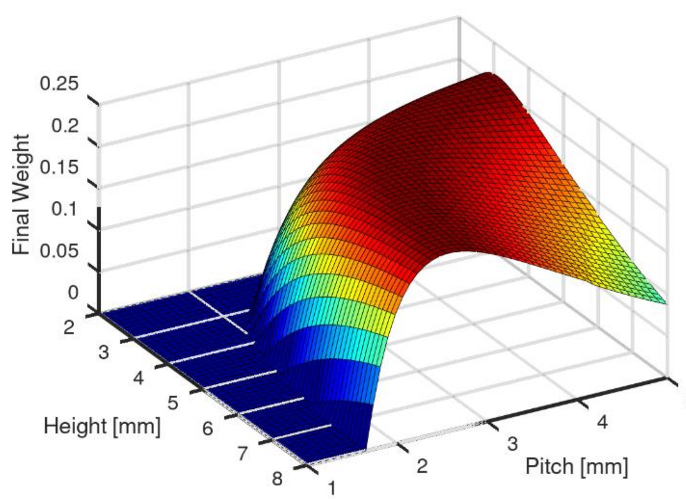

Figure 20: Final weight ratio surface contour.

DOI: 10.17185/duepublico/77298

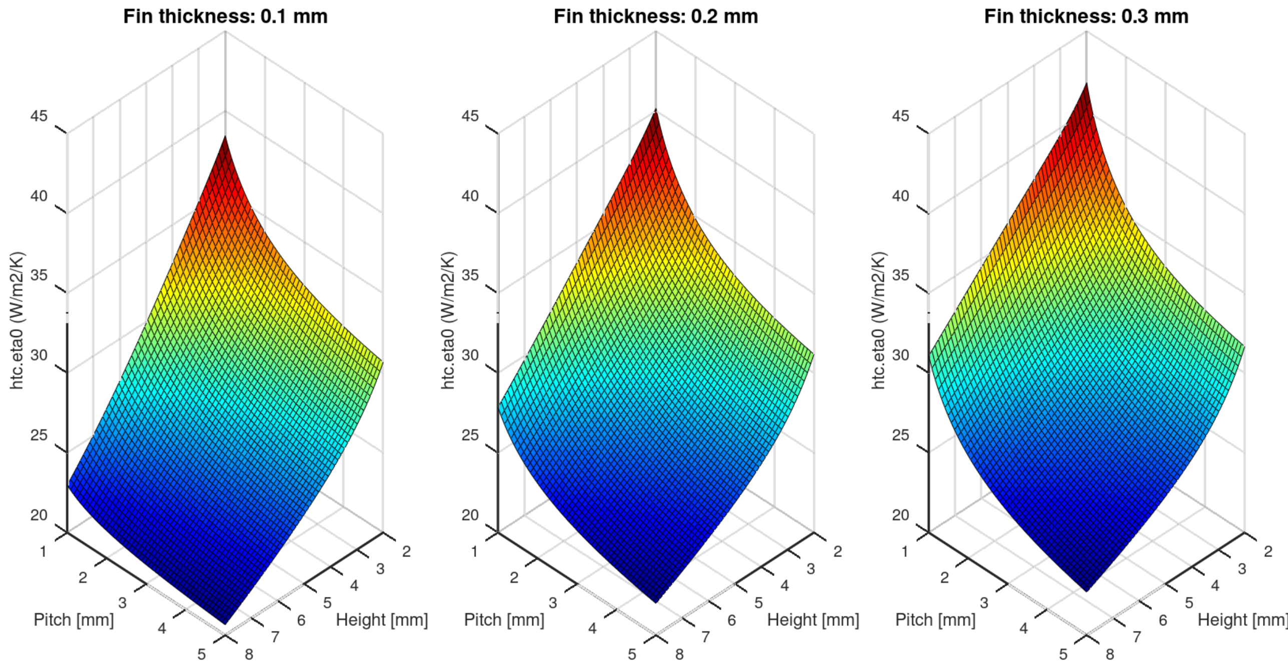

Figure 21: Comparison of an effective heat transfer coefficient for different fin thicknesses

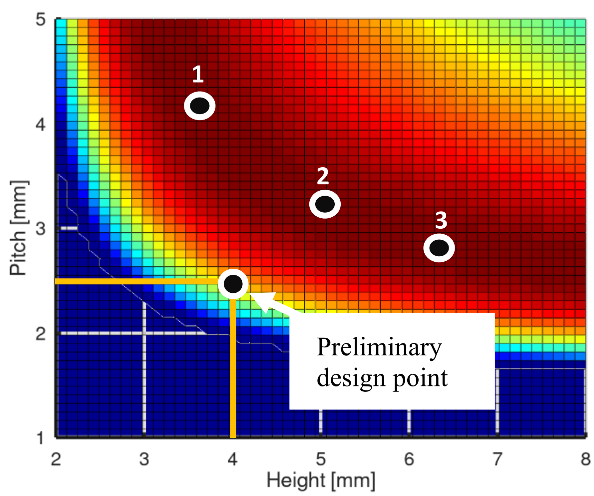

Figure 22: Final weight ratio surface contour - top view.

Table 4: Air channel optimisation points.

	P (mm)	**H (mm)**	**H/P**	**htc.n$_0$ (W/m^{2}K)**	**Δp (Pa/m)**
Preliminary design	2.54	4	1.57	32.2	412
1	4.2	3.7	0.88	28.5	257
2	3.2	5	1.56	28.7	265
3	2.8	6.3	2.25	29	276

CONCLUSION

The present work contains findings and results from the experimental campaign, verifying the thermal–hydraulic design of the plate and fin heat exchanger (PFHE) mock-up, which was designed and fabricated in the framework of the Horizon 2020 sCO2-4-NPP project. The preliminary PFHE concept was designed to exchange the heat between air and sCO_2, where the sCO_2 side was operated at 8 MPa of pressure and a temperature range of <100; 172°C>. The main findings include the heat transfer and the fanning friction coefficients correlations on the air of the PFHE. Furthermore a 1D mathematical model was proposed and validated with the experimental data. Based on the results, an optimisation study of the air channels was made to find the channel geometry with optimal heat transfer and sufficiently low pressure losses. The results of this study show that increasing the fin thickness has a positive effect on the increase of the heat transfer coefficient. Moreover, an optimum field of the optimised parameters exists, for the given boundary conditions. Data points from this optimum field show a slight decrease in heat transfer coefficient compared to the preliminary design; however, they show in average up to 35% lower pressure losses.

DOI: 10.17185/duepublico/77298

ACKNOWLEDGEMENTS

This project has received funding from the Euratom research and training programme 2014-2018 under grant agreements No 662116 (sCO$_2$-Hero), No 764690 (sCO$_2$-Flex) and No 847606 (sCO$_2$-4-NPP).
The presented results were obtained using the CICRR infrastructure, which is financially supported by the Ministry of Education and Culture - project LM2023041

DISCLAMER

This text reflects only the author's view and the Commission is not liable for any use that may be made of the information contained therein.

NOMENCLATURE

A	Total heat transfer area; m^2
A_f	Fins heat transfer area; m^2
c_p	Isobaric heat capacity; J/(kg.K)
D_H	Hydraulic diameter; m
f	Fanning friction coefficient; (-)
G	Mass-flow per flow cross-section; kg/(s.m^2)
H	Channel height; m
i	Enthalpy; (J/kg)
j	Colburn factor; (-)
k	Thermal conductivity; W/(m.K)
K_c	Entrance friction factor; (-)
K_e	Exit friction factor; (-)
L	Effective length; m
$\dot{m}$	Mass flow; kg/s
Nu	Nusselt number; $Nu = h.D_p/k_f$ (-)
N	Number of channels; (-)
Re	Reynolds number; $Re_p = v\, \rho\, D_p/\mu$ *(-)*
R	Thermal resistance; W/(m^2.K)
p	pressure; (Pa)
P	Channel Pitch; m
Pr	Prandtl number; $Pr = c_f.\mu/k$ (-)
Q	Transferred heat; W
T	Temperature; °C
U	Over all heat transfer coefficient; W/(m^2.K)
t	Fin thickness; m
v	Flow velocity; m/s
W	Flow heat capacity; W/K
Greek letters	
ε	Heat exchanger effectiveness; (-)
Δ	Difference
ρ	Density; kg/m^3
μ	Dynamic viscosity; Pa.s
η_0	Total surface effectiveness; (-)
η_f	Fin efficiency; (-)
σ	Contraction/expansion ratio
Acronyms and abbreviations	
BWR	Boiling water reactor
DUHS	Diverse ultimate heatsink
htc	Heat transfer coefficient, W/(m^2.K)
HX	Heat exchanger
LMTD	Logarithmic mean temperature difference; °C/K
NTU	Net transfer unit; (-)
FPM	Fins per meter
PFHE	Plate and fin heat exchanger
PID	Piping and instrumentation diagram
SBO	Station blackout
Subscripts	
s	Solid
m	Mean value
i	Inlet/rows in array
o	Outlet

REFERENCES

[1] "sCO2-4-NPP." https://www.sco2-4-npp.eu/ (accessed Aug. 09, 2022).

[2] A. Vojáček, "SCO2 EXPERIMENTAL LOOP AND CVR R&D ACTIVITIES," Sep. 01, 2017. http://www.sco2-hero.eu/wp-content/uploads/2017/09/03_Vojacek_CVR_sCO2-experimental-loop-and-CVR-RD-activities.pdf (accessed Aug. 09, 2022).

[3] J. Venker, "Development and validation of models for simulation of supercritical carbon dioxide Brayton cycles and application to self-propelling heat removal systems in boiling water reactors," 2015.

[4] E. W. Lemmon, and Ian H. Bell, M. L. Huber, and M. O. McLinden, "NIST Standard Reference Database 23: Reference Fluid Thermodynamic and Transport Properties-REFPROP, Version 10.0, National Institute of Standards and Technology." 2018. doi: https://doi.org/10.18434/T4/1502528.

[5] V. Gnielinski, "Heat Transfer in Pipe Flow," in *Heat Atlas VDI*, 2010, pp. 693–699.

[6] A. P. Colburn, "A method of correlating forced convection heat-transfer data and a comparison with fluid friction," *Int J Heat Mass Transf*, vol. 7, no. 12, pp. 1359–1384, Dec. 1964, doi: 10.1016/0017-9310(64)90125-5.

[7] W. M. Rohsenow, James. P. Hartnett, and Y. I. Cho, "Heat exchangers," in *Handbook of heat transfer*, 1993, pp. 1277–1308.

[8] W. M. Kays and A. L. London, *Compact Heat Exchangers, 3rd edition*. New York: McGraw-Hill, 1998.

DOI: 10.17185/duepublico/77298

Appendix A

Exp.	F_air (m3/h)	Δp_air (Pa)	Tin_Air (°C)	Tout_Air (°C)	MF_CO2 (kg/s)	Pabs_CO2 (MPa)	Δp _CO2 (Pa)	Tin_CO2 (°C)	Tout_CO2 (°C)
1	18.15	18	20.3	84.4	0.0708	8	6340	101.6	98.2
2	122.4	133	20.3	70.3	0.0708	8	6100	102.2	86
3	235	322	21	59.2	0.0708	8	5830	103.3	80.2
4	339	620	21.8	55.1	0.0708	8	5750	104	74.3
5	455	1065	22.7	51.5	0.0708	8	5680	105.7	70.5
6	17.8	19	23	91.6	0.11	8	11400	108.5	105.2
7	120	134.5	21.4	77.2	0.11	8	11000	109	94.6
8	234	326	21.4	63.8	0.11	8	10480	109	88.1
9	336	625	21.9	60	0.11	8	10730	110.4	83.2
10	455	1080	23.2	57	0.11	8	10900	111.8	80
11	62	66	21.6	93.5	0.14	8	20200	112.7	104.5
12	119	135	21.7	82.5	0.14	8	19300	112.7	100.5
13	232	330	21.4	67	0.14	8	18700	112.5	94.5
14	335	630	21.7	62.8	0.14	8	17650	112.7	88.4
15	455	1080	22.5	58	0.14	8	16600	112.5	83.2
16	59	67	22.8	115.5	0.07	8	8900	142.2	126.6
17	128	156	22.1	93.8	0.07	8	7480	141.3	115.4
18	230	336	22.6	72.6	0.07	8	6540	135.5	99.6
19	344	670	23.3	66.5	0.07	8	6180	138	90.8
20	450	1085	22.7	61.6	0.07	8	6410	137	85
21	157	225	23	108	0.11	8	14400	172.2	140.6
22	242	406	23.3	93.8	0.11	8	13900	171.8	133
23	310	603	23.9	86.5	0.11	8	13500	171.6	125.1
24	379	852	24.1	82.7	0.11	8	13200	171	118.1
25	455	1183	25	78.3	0.11	8	13100	170	112.7
26	455	1160	25	73.1	0.081	8	7800	170	102.2
27	380	846	24.1	77.1	0.081	8	7840	170	106.9
28	304	567	23.9	81.3	0.081	8	8000	170	114.8
29	201	305	23.4	93.9	0.081	8	8450	171.3	127
30	81	104	23.6	123.5	0.081	8	9400	172.5	143.6

DOI: 10.17185/duepublico/77298

DOI: 10.17185/duepublico/77298
URN: urn:nbn:de:hbz:465-20230427-135329-4